J. Fluid Mech. (2009), *vol.* 628, *pp.* 1–21.
doi:10.1017/S0022112009005825 Printed in the United Kingdom

Dam-breaking seiches

N. J. BALMFORTH[1], J. VON HARDENBERG[2] AND R. J. ZAMMETT[3]†

[1]Department of Mathematics and Department of Earth & Ocean Science, University of British Columbia, Vancouver, BC V6T 1Z2 Canada

[2]Institute of Atmospheric Sciences and Climate, CNR, 73100 Lecce, Italy

[3]Department of Mathematics, University of Oxford, 24–26 St Giles, Oxford OX1 3LB, UK

(Received 30 March 2008 and in revised form 2 January 2009)

Experimental and theoretical models are used to explore the break of a moraine dam by catastrophic erosional incision initiated by an overtopping wave. The experiments are conducted in a rectangular tank with an erodible barrier made from sand and grit. Theory combines shallow-water hydrodynamics with an empirical model of erosion. The models confirm that dams can be broken by a catastrophic incision. However, the displacement wave does not break the dam in its first passage but excites a long-lived seiche that repeatedly washes over the dam. The cumulative erosion of the downstream face by the overtopping seiches eventually allows an incipient channel to form, and catastrophic incision follows. Estimates are presented of the strength of the initial disturbance required to break the dam, the maximum discharge and the duration of the runaway incision.

1. Introduction

Geological records suggest that a number of recent floods have originated from lakes dammed by glacial moraines and been caused by a catastrophic erosional incision of the dam, triggered by either overfilling during unusual weather conditions or a large overtopping wave (Clague & Evans 2000). The moraine which dammed Lake Tempanos in Argentina, for example, failed in the 1940s due to meltwater accompanying a retreat of the glacier (Rabassa, Rubulis & Suarez 1979). On the other hand, large destructive waves can be generated by ice or rock falls, which are likely in steep alpine valleys or beneath the unstable toe of a retreating glacier. For example, a rock avalanche into the glacial lake Safuna Alta created a displacement wave over 100 m high (Hubbard *et al.* 2005), and although the dam did not break, the wave did generate significant erosion.

A catastrophic erosional incision can be triggered when overfilling or an overtopping wave notches an incipient channel at the top of the dam; the increased flow through that opening erodes and deepens the channel still further, which accelerates the outflow and the erosion, leading to a runaway incision. Artificial earthen dams are known to fail in this fashion when the adjoining reservoir is overfilled, and various theoretical and experimental models of the process have been constructed (e.g. Walder & O'Connor 1997; Coleman, Andrews & Webby 2002; Cao *et al.* 2004). By contrast, the failure of a moraine-dammed lake has never been directly witnessed, and triggering

† Email address for correspondence: rachel_zammett@yahoo.co.uk

incision with a large overtopping wave has not previously been modelled in any detail. The purpose of the current study is to provide the first such models.

Our approach is on the idealized side, combining experimental and theoretical modelling, and expands substantially on the preliminary work reported by Balmforth *et al.* (2008). The experiments are conducted in a smaller scale laboratory setting, in which the geometry of the lake-moraine system is roughly reduced proportionately. Unfortunately, we are unable to similarly scale down either the material properties of the erodible dam or the dynamics of the turbulent water flow. Part of the difficulty is the lack of detailed information on the material properties of glacial moraines (but see Clarke 1987; Clague & Evans 2000), and to reproduce the turbulent dynamics, we would require a bigger apparatus. Thus, the experiments are not in the same dynamical regime as the geological problem. Instead, we have opted for a simpler, more qualitative approach, which can make a firmer contact with the accompanying theory.

The theory couples shallow-water equations for the fluid flow with an empirical erosion law that determines the height of the dam. For simplicity, the model is two-dimensional, describing the structure of the flow and the bed in a plane perpendicular to the dam. This restriction signifies that we cannot capture the fully three-dimensional dynamics of channelization. Balmforth *et al.* (2008) presented a short theoretical discussion of such three-dimensional dynamics, and we comment in more detail on the ramifications of the restriction to two dimensions later in the current paper.

Guided by both the theory and experiments, we also outline a much simpler mathematical model of the dam-break dynamics. This reduced model can be used to gauge in a convenient and simple setting the effect of the various physical parameters of the problem. Moreover, in principle, the model can be straightforwardly extended to add a number of physical processes that we currently ignore and to explore the motivating geophysical application.

Overall, the thrust of our study is to explore under what conditions a wave can initiate runaway incision and break a dam. We also examine properties of the resulting flood, such as the maximum discharge and the duration of the dam break. In principle, these results bear on the important issues of outburst probability and hazard control and mitigation (McKillop & Clague 2007*a*, *b*). There are also applications to understanding the release of sediments during the dam break (Cui *et al.* 2006*a, b*).

2. Experiments

The experiment consists of a rectangular glass tank with length 125 cm and depth 30 cm. The width of the tank was 20 cm, but by inserting a second panel it could be reduced to 5 cm. The downstream end of the tank was open to allow water and sediment to drain from the tank. The dams were built from the materials described below and were shaped into a roughly Gaussian profile, using an appropriately shaped stencil, with heights of about 10 cm and half-widths (standard deviations of the Gaussian) of 10 cm. The dams were positioned to leave a metre-long reservoir that was filled with water up to a depth close to the top of the dam, and the obstruction was left for a time to allow some water to seep through and check that the dam could withstand the upstream water pressure. (Some images showing the dammed reservoir through the sidewall of the tank appear in figures 1–4.) A wave was then initiated in the reservoir by sweeping water towards the dam using a paddle. A video camera captured the resulting action. From the video images we extracted profiles of the dam

Sediment	ρ (g cm^{-3})	Porosity	Modal particle size (μm)	Angle of repose
Medium sand	2.34	0.38	310	36°
Coarse sand*	2.34	0.35	950	36°
Grit	2.42	0.42	1150	34°
Fine sand/grit mix*	2.38	0.32	250 and 1150	36°
Medium sand/grit mix*	2.36	0.37	310 and 1150	38°

TABLE 1. Properties (when dry) of the individual sediments and mixes that were used to build the dams; the stars indicate which materials made stable but erodible dams. Modal particle size was estimated from distributions obtained by laser diffraction. The angles of repose are estimated by tilting or building up a pile of sediment.

and water depth; by floating tracer particles on the water surface we estimated flow speeds.

Glacial moraines are poorly sorted and loosely consolidated sediments with particle sizes ranging from fine clays to large boulders, and some evidence for a bimodal particle size distribution (Clarke 1987). Accordingly, we used a variety of experimental materials to construct the dams: three types of sand and a coarser grit, each of which individually was roughly modal. The sands had different mean diameters (motivating references to 'fine', 'medium' and 'coarse') and relatively wide particle size distributions. The grit consisted of larger particles of roughly equal size. To make sediments with bimodal particle size distributions, we mixed the grit with one of the sands in roughly equal proportions. The materials, their mean particle sizes and some other properties are listed in table 1.

Not all the materials listed in table 1 were suitable for building dams: those built from the medium sand were unable to withstand the upstream water pressure and broke before a wave was even initiated. (The fine sand by itself was even worse, and so this material was used only in the mixtures.) The grit made a very porous obstruction, and water drained quickly through, leading to waterlogged structures in which the downstream face eventually mobilized and collapsed. It was also hard to incise a channel in the grit dams because the overtopping water often seeped into the dam rather than eroding it. Overall, the coarse sand and the two sand/gravel mixtures proved to be the best materials, in terms of providing a dam that was both stable and erodible by overtopping waves. We speculate that this is because all three materials contained roughly equal amounts of relatively large and small particles: the larger particles contributed to dam stability, whilst the smaller particles blocked the seepage through the structure and allowed greater erodibility.

Provided the amplitude of the initial disturbance was sufficiently strong, and the dam was made of suitable material (those denoted by stars in table 1), we were able to initiate runaway incisions. These dam breaks invariably began with a large wave overtopping the dam and eroding a significant fraction of the downstream face. However, in none of the experiments was that wave able to create an incipient channel to trigger a catastrophic incision. (Overly strong waves caused a mechanical failure of the whole structure.) Instead, a large fraction of the wave energy was reflected back into the reservoir, and fairly quickly a seiche (sloshing) emerged that repeatedly overtopped the dam. Each overtopping contributed to the erosion of the downstream face of the dam, plus some removal of material from its peak. Eventually, the incipient channel was cut, and a catastrophic incision followed that emptied the majority of the reservoir within a minute.

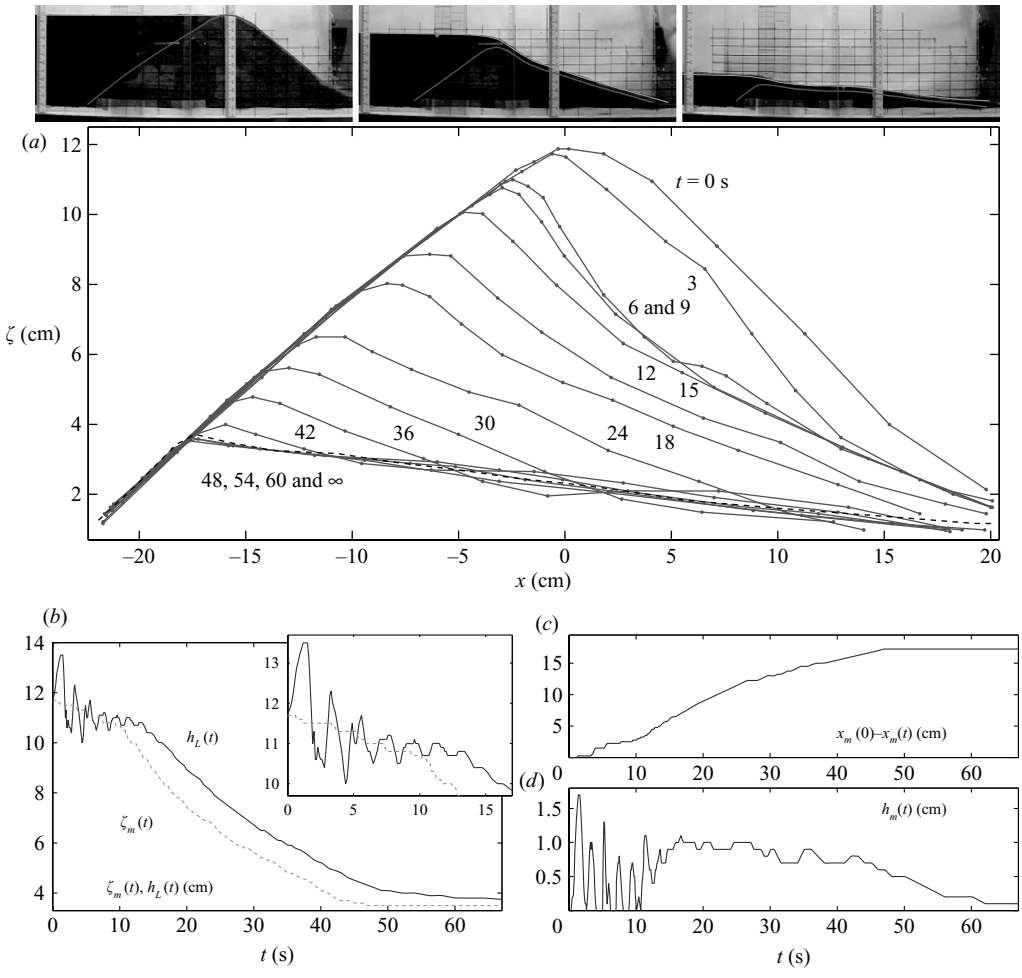

FIGURE 1. A successful dam break in the narrow tank. Shown in panel (*a*) are three photographs (at $t = 0$, 18 and 45 s) plus a sequence of curves plotting the dam profile at the times indicated. The wedge-shaped final state to which the eroded dam converges is shown by the dashed line. The lower panels show (*b*) the reservoir depth (measured at the left side of the photographs), $h_L(t)$, and maximum dam height, $\zeta_m(t)$, (*c*) the shift in the position of the dam's maximum, $x_m(0) - x_m(t)$, and (*d*) the water depth at that maximum, $h_m(t)$.

Figures 1 and 2 show examples of successful dam breaks in the narrow (5 cm) and wide (20 cm) tank, respectively, for dams made from the coarse sand. The figures display the evolving profile of the dams, together with time series of a number of quantities that play a key role in later theoretical developments: the dam's maximum height and position, the water depth in the reservoir and the water depth at the dam maximum. The reservoir depth is measured just upstream of the dam (at the left of the photographs in figures 1 and 2). More examples are presented in figure 3, which compares the evolution of reservoir depth for several experiments in wide and narrow tanks and with two different materials for the dams.

An important difference between the dam breaks in figures 1 and 2 is that the dam in the narrow tank erodes in an almost two-dimensional fashion, whilst the obstruction in the wide tank is channelized by the overtopping waves (as in the example presented

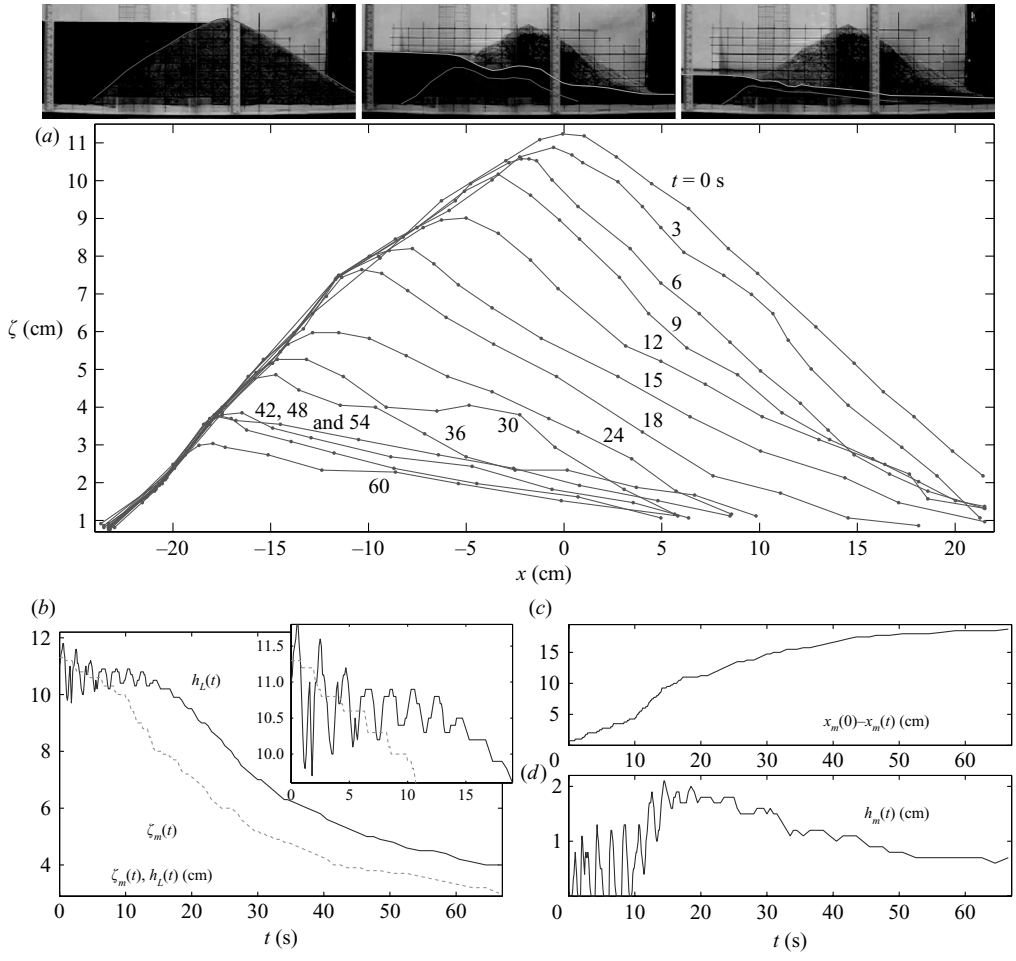

FIGURE 2. A successful dam break in the wide tank. Shown in panel (*a*) are three photographs (at $t = 0$, 30 and 60 s), plus a sequence of curves plotting the dam profile at the times indicated, as measured from the bed of the outflow channel (revealed in the foreground of the photographs). The lower panels show (*b*) the reservoir depth, $h_L(t)$, and maximum dam height, $\zeta_m(t)$, (*c*) the shift in the position of the dam's maximum, $x_m(0) - x_m(t)$, and (*d*) the water depth at that maximum, $h_m(t)$.

by Balmforth *et al.* 2008). The resulting breach allows observation of the depth and bed of the eroding outflow channel if the channel forms adjacent to one side of the tank (see the photograph inset into figure 3), which could be engineered by slightly lowering the dam on that side at the outset. In figure 2, the largely uneroded parts of the initial dam are visible in the background, and the dam profiles and maximum height correspond to the bed of the outflow channel, revealed in the foreground. For both narrow and wide tanks, the fluid flow primarily erodes the downstream flank of the dam; towards the end of the experiments the erosion slows as the reservoir level declines, leaving intact a shallow, wedge-shaped structure whose upstream face is a relic of the original dam.

If the amplitude of the initial disturbance was too weak, a runaway incision did not occur: although an overtopping seiche could be excited in the reservoir, that motion eventually damped away before a channel was cut into the top of the dam.

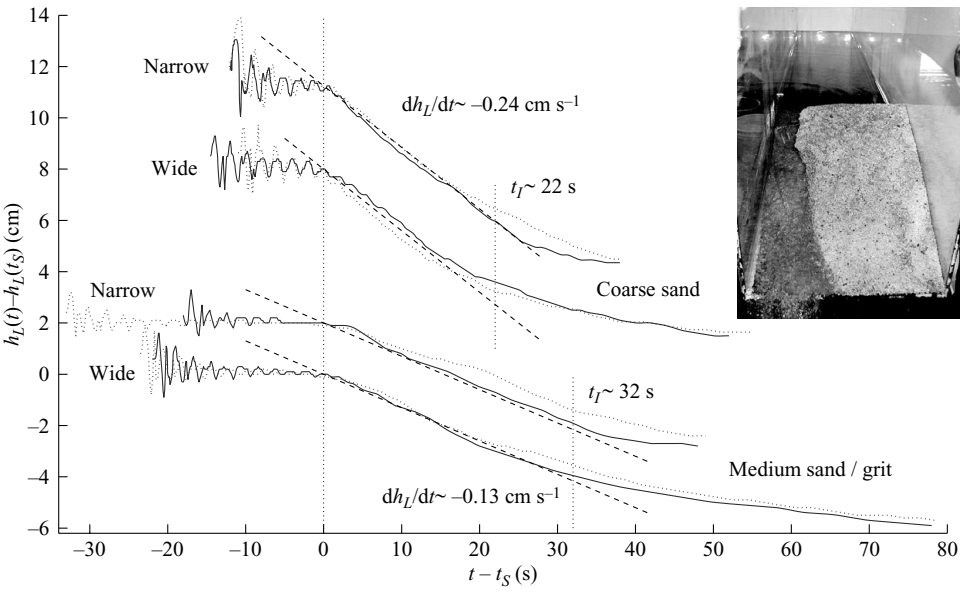

FIGURE 3. Plots of reservoir depth against time for dams constructed of coarse sand and the medium sand/grit mix. For each sediment, two experiments are displayed for both wide and narrow tanks. The origin of time is shifted to the moment that the incipient channel forms (denoted t_S), and the change in depth from that moment is plotted (i.e. $h_L(t) - h_L(t_S)$ against $t - t_S$). The curves for the different pairs of experiments are offset from one another for clarity, and lines showing characteristic values of dh_L/dt are also added. Estimates for the duration of the incision, denoted t_I, are indicated (determined as the interval over which $|dh_L/dt|$ is near its maximum). The inset shows a photograph of an incised dam of coarse sand in the wide tank.

An example of such an 'unsuccessful' dam break is shown in figure 4. Evidently, the initial wave must be sufficiently strong so that the seiche can repeatedly spill over the dam and cut an incipient channel, before dissipation saps its strength and drainage lowers the reservoir level. When the seiche did not spill over the dam, the decay of its amplitude took an exponential form and could be reproduced by Keulegan's (1959) viscous boundary layer model, indicating that dissipation inside Stokes layers adjacent to the walls was primarily responsible. (This theory is compared with numerical results in figure 6 and further discussed in § 5.2.) On the other hand, the decay was stronger when the seiche spilled over the dam, suggesting that transmission of wave energy also played a role. In view of the simple method used to generate the initial disturbance, we did not study in detail the implied amplitude threshold. Nevertheless, by extracting initial wave amplitudes from the video recordings, we estimated that, for the coarse sand dams shown in figures 1 and 4, the threshold, as measured by the elevation of the water surface, was about 12 % of the reservoir depth.

An interesting feature of the results shown in figure 3 is that the dam break is very similar in both narrow and wide tanks (compare also figures 1 and 2). In view of the different nature of the incision in the two cases (two-dimensional versus channelized), the apparent insensitivity to the width is surprising. Indeed, the widths of breaches varied significantly in experiments in the wide tank with the same dam materials and comparable initial conditions (for example, the two experiments with coarse sand presented in figure 3 formed breaches whose maximum widths differed by almost

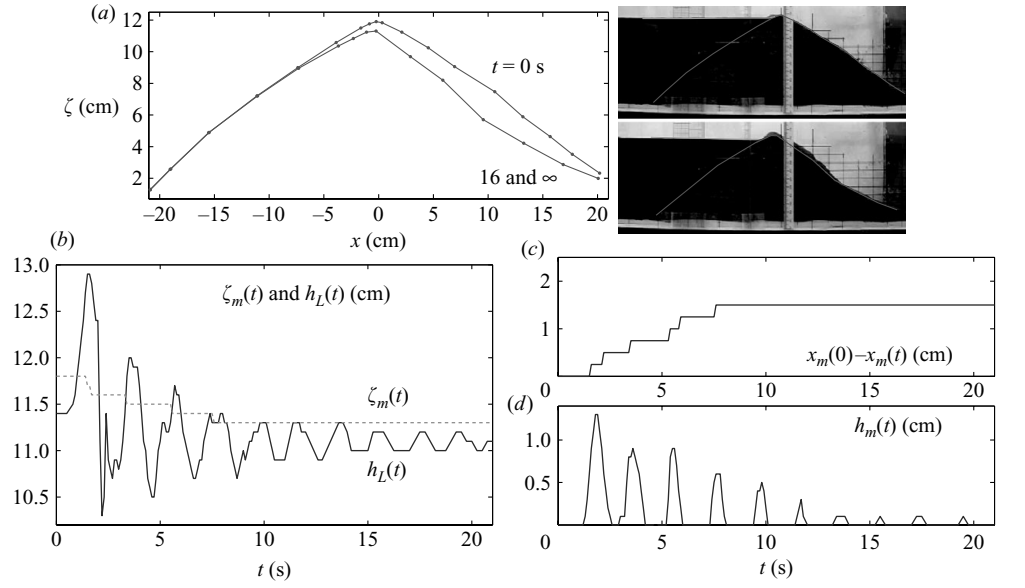

FIGURE 4. An unsuccessful dam break in the narrow tank. Shown in panel (*a*) are the initial and final dam profiles. The lower panels show (*b*) the reservoir depth, $h_L(t)$, and maximum dam height, $\zeta_m(t)$, (*c*) the shift in the position of the dam's maximum, $x_m(0) - x_m(t)$, and (*d*) the water depth at that maximum, $h_m(t)$.

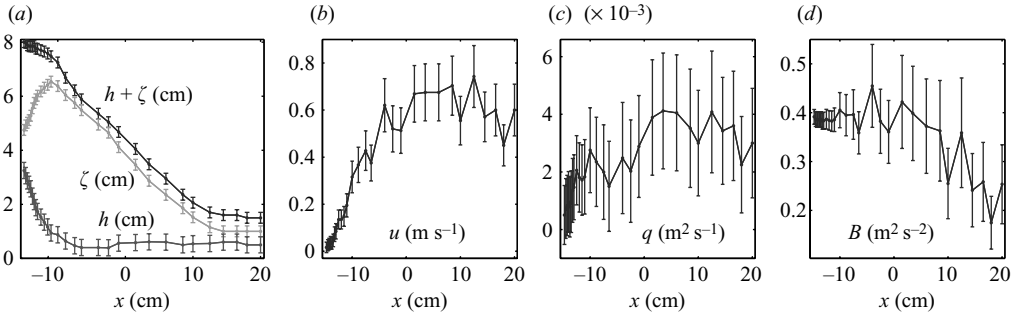

FIGURE 5. Flow measurements following a tracer particle moving through the breach during the dam break of figure 1. Plotted against tracer position (with the origin located at the original maximum elevation of the dam) are (*a*) the free surface, $h + \zeta$, maximum dam height, ζ, and water depth, h, (*b*) speed, u, (*c*) flux, $q = hu$, and (*d*) $B = g(h + \zeta) + u^2/2$. The error bars reflect errors in the measurement of position.

a factor of two), yet the incision rates remained very similar. In contrast, the dam composition is much more significant: the coarse sand dams erode significantly faster.

Finally, figure 5 shows some extra details of the flow dynamics during the catastrophic incision in the experiment of figure 2. The picture displays the dam height ζ, water depth h and speed u as one moves through the breach in the dam, obtained by following the position of a tracer on the water surface. From these measurements, the flux hu and 'Bernoulli potential' $B = g(h+\zeta)+u^2/2$ are calculated, which play an important role in the theoretical developments to follow. There is some suggestion that both hu and B are roughly constant moving with the particle, but the data are not very conclusive because the estimates of speed u are not very precise.

3. A shallow-water model

3.1. *Governing equations*

To model the dam break dynamics, we use the shallow-water equations, modified to include dissipative terms and supplemented with an equation for the erodible bed. The main variables are the local water depth $h(x,t)$ and speed $u(x,t)$ and the bed elevation $\zeta(x,t)$. The erodible material is piled up to form a dam on top of the x-axis, which is taken to be immobile (and impermeable), so $\zeta > 0$. The model is the two-dimensional version of that described by Balmforth *et al.* (2008), and the reader is referred to that paper for additional details.

We express the equations in a dimensionless form by scaling horizontal lengths by the dam's characteristic width, Δ (the standard deviation of its Gaussian shape, $\Delta = 10$ cm in the experiments), vertical lengths by the initial dam height Z_0, speeds by $\sqrt{gZ_0}$ and time by $\Delta/\sqrt{gZ_0}$ (g being gravitational acceleration). The shallow-water equations are then

$$h_t + (hu)_x = 0, \tag{3.1}$$

$$u_t + uu_x = -h_x - \zeta_x - (c_f|u| + \lambda)\frac{u}{h} + \nu u_{xx}, \tag{3.2}$$

where the subscripts x and t denote partial derivatives. The final three dissipative terms on the right of (3.2) contain three dimensionless parameters, which can all be written alternatively in terms of dimensional constants:

$$c_f = \frac{\Delta C_f}{Z_0} \qquad \text{and} \qquad \nu = \frac{\nu_T}{\Delta\sqrt{gZ_0}}, \qquad \lambda = \frac{\Lambda\Delta}{Z_0\sqrt{gZ_0}}. \tag{3.3}$$

Thus, C_f denotes a Chézy coefficient parameterizing turbulent bottom drag; ν_T is a kinematic viscosity representing turbulent eddies; and Λ is a laminar friction factor (with units of m s^{-1}). The turbulent parameterizations are relevant in the geological problem, whereas laminar friction is introduced to model viscous Stokes layers in the laboratory setting. The diffusion term in (3.2) takes a simple viscous form but is not conservative, which requires a term of the form $\nu h^{-1}(hu_x)_x$. Both forms have been explored in the literature (e.g. Needham & Merkin 1984; Merkin & Needham 1986), always with the goal of smoothing the solution; we used the non-conservative form in the computations reported below, although we did verify that computations with the conservative version did not lead to significantly different results.

We use an Exner equation for the bed elevation,

$$\zeta_t = -\epsilon E(u^2), \tag{3.4}$$

which contains a dimensionless erosion parameter ϵ and a function that depends on the stress exerted on the bed by the water (given dimensionlessly by u^2). We take

$$E(u^2) = \begin{cases} 0, & u^2 < u_*^2, \\ (u^2 - u_*^2)^\alpha, & u^2 \geqslant u_*^2, \end{cases} \qquad u_* = U_*/\sqrt{gZ_0}, \tag{3.5}$$

and

$$\epsilon = \frac{W\Delta}{Z_0}(gZ_0)^{\alpha-1/2}, \tag{3.6}$$

where U_* denotes a (dimensional) threshold speed below which erosion does not take place; W is the dimensional counterpart of ϵ; and α is an empirically determined parameter that we fix equal to 3/2 (cf. Parker 2006). This formulation for erosion was

used by Cao *et al.* (2004) and Taki & Parker (2004), amongst others, although the choice of α may not be appropriate for steep slopes (Rickenmann 2001).

Equation (3.4) accounts only for erosion but not deposition. Sedimentation effects can be incorporated into the model by including an additional variable representing the concentration of suspended load (see Balmforth *et al.* 2008). Alternative flux formulae may also be more appropriate when bed load transport dominates the sediment transport (e.g. Parker 2006). Indeed, whereas observationally it was clear that sediment was being transported within the bulk of the fluid during the fastest phases of the dam break once the incision slowed, bed load dominated the transport. (The water column was visibly clouded by suspended sediment; the importance of suspended load is confirmed by estimates of the Rouse and Shields numbers, which, for the coarse sand experiments, are of the order of one and three respectively, using the fluid speeds of $U_m = 0.2\,\mathrm{m\ s^{-1}}$, which we measured close to the top of the dam (compare with figure 5).) Thus, although our transport law may apply for parts of the dam break, it is not clear that the law is very accurate in the later stages. In the interest of brevity, we omit such generalizations of the model and note only that we have verified that the qualitative details of the dam break dynamics predicted by the model is not dictated by the specific model of erosion. Also, the shallow-water equations in (3.1)–(3.2) ignore any sources of mass and momentum in the fluid equations due to erosion and deposition. This simplifying approximation is standard but known to be inaccurate in some related contexts (Cao *et al.* 2004). Elsewhere (Balmforth *et al.* 2008), we found that including the feedback of the sediment on the water flow had no qualitative effect. Finally, our sediment is implicitly taken as uniform, so we do not account for a bimodal particle distribution or further complications of the sediment dynamics.

We solve the system (3.1)–(3.2) and (3.4) numerically in the domain $0 < x < 2\ell$ beginning from an initial condition corresponding to a dammed lake with a superposed wavy disturbance. The maximum of the initial dam is positioned at $x = \ell$, with the reservoir occupying the region $0 < x < \ell$. (So ℓ is the dimensional lake length in units of the dam width: $\ell = L/\Delta$.) We take

$$h(x,0) = h_{eq}(x) + A_0 \sin(2\pi x/\ell), \qquad u(x,0) = 0, \qquad \zeta(x,0) = \mathrm{e}^{-\frac{1}{2}(\ell - x)^2}, \tag{3.7}$$

$$h_{eq}(x) = \begin{cases} h_0 - \zeta(x), & h_0 > \zeta \text{ and } x < \ell, \\ 0, & \text{otherwise}, \end{cases} \tag{3.8}$$

where h_0 and A_0 are parameters. That is $\zeta(x,0)$ and $h_{eq}(x)$ represent the undisturbed lake, whose level is a fraction h_0 of the dam height; the wave is launched by perturbing the lake depth with a sinusoidal disturbance of amplitude A_0. For boundary conditions, we take $u = h_x = 0$ at $x = 0$ (an impermeable wall) and impose 'open' flow conditions $u_x = h_x = 0$ at $x = 2\ell$. The numerical technique used is described further in Balmforth *et al.* (2008).

3.2. *Numerical results*

Figure 6 presents two sample numerical solutions with different initial wave amplitudes. Shown is the evolution of the water surface $h(x,t) + \zeta(x,t)$ in space and time, a time series of the dam height $\zeta_{max}(t)$, water depth at the left boundary of the reservoir $h(0,t)$ and a series of snapshots of the dam profile. In each case, the initial disturbance generates waves that subside into a regular seiche. The spilling of the seiche over the dam generates pulses in discharge that sequentially lower the

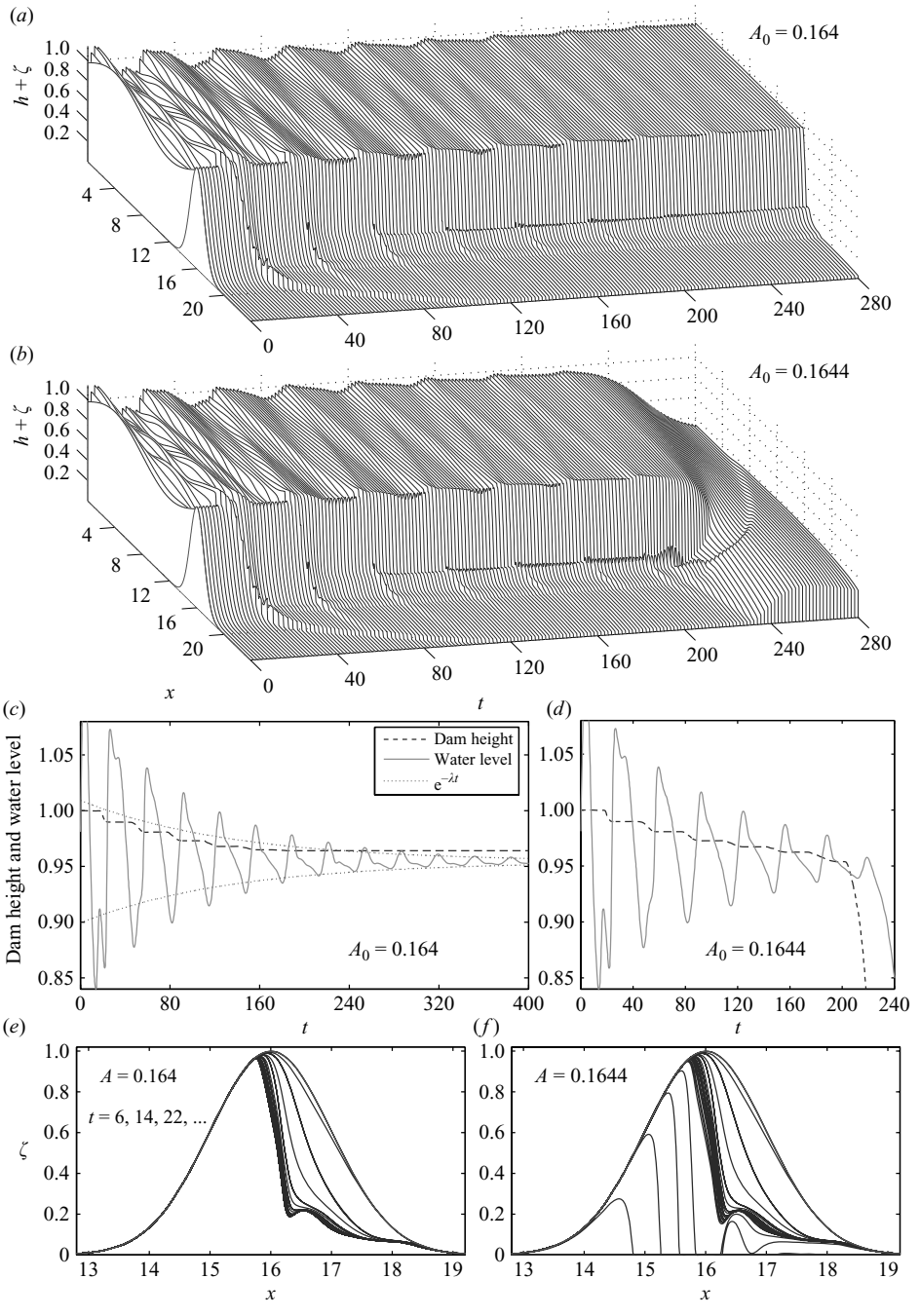

FIGURE 6. Two numerical solutions of the shallow-water model with initial wave amplitudes of $A_0 = 0.164$ and 0.1644. The elevation of the water surface, $h(x,t) + \zeta(x,t)$, is shown in panels (a) and (b) as a surface over the (t,x)-plane. Panels (c) and (d) show the dam height, $\zeta_{max}(t)$, and the water level at the left boundary of the upstream basin, $h(0,t)$, against time. Panels (e) and (f) show the evolution of the dam profiles. In panel (c), the expected exponential decay (with exponent $\gamma \simeq 0.0074$) of the linear seiche is also shown. The parameter settings are $\epsilon = 0.25$, $u_* = 0.1$, $\nu = 0.04$, $c_f = 0.0125$, $\ell = 16$, $\alpha = 3/2$, $h_0 = 0.98$ and $\lambda = 0.0125$, and there are 2048 gridpoints in x. These parameters are similar to the experimental parameters, whose calibration is discussed in § 5.2.

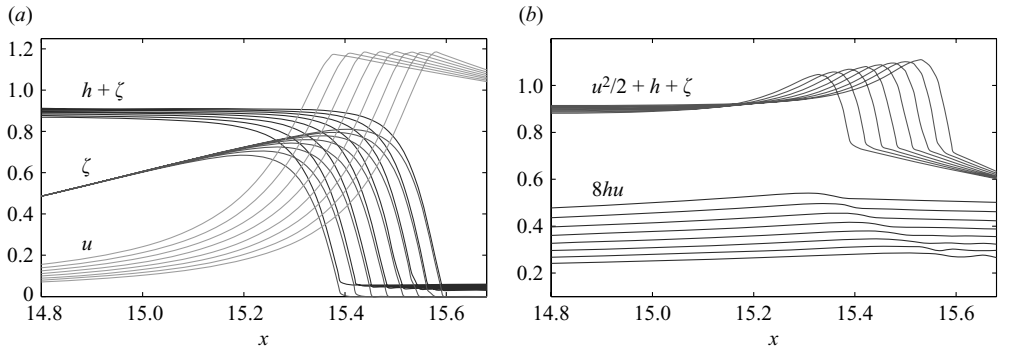

FIGURE 7. Snapshots of (*a*) $h+\zeta$, ζ and u and (*b*) $8q=8hu$ and $B=u^2/2+h+\zeta$ during the runaway incision of the dam break computation shown in figure 6. (The snapshots are 0.8 time units apart.)

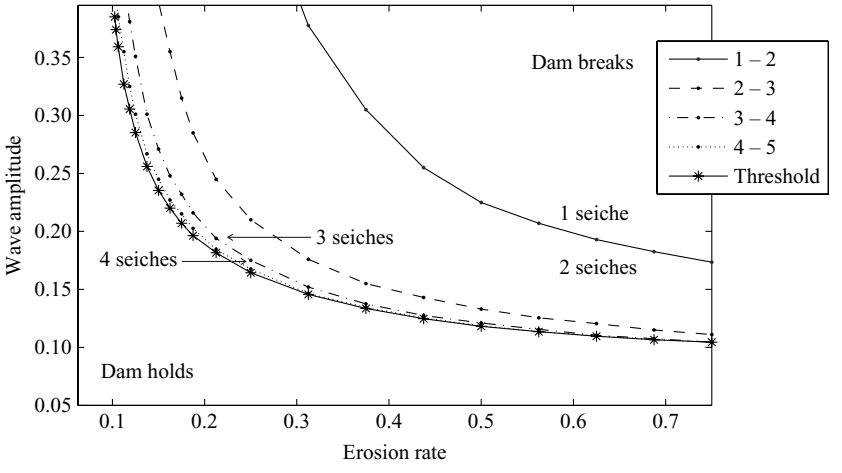

FIGURE 8. The threshold for the dam break on the (ϵ, A_0)-plane; the remaining parameter settings are as in figure 6. Also indicated are the divisions between regions in which different numbers of seiches are required to break the dam.

barrier. The higher amplitude initial wave ultimately breaks the dam after about seven periods of the seiche. The weaker disturbance, however, damps away to leave the obstruction intact; once overtopping subsides, the seiche decays exponentially with the rate expected for the linear normal mode (see figure 6*c*). Note the sharp shock-like features that propagate downstream of the dam after each overtopping, which is typical of shallow-water hydraulics in this type of situation. These weak bores are diffusively smoothed and have speeds that are influenced by the viscous term added to the shallow-water equations (e.g. Merkin & Needham 1986).

More details of the breaching process are displayed in figures 7 and 8. The first figure shows the flux, $q=hu$, and (dimensionless) Bernoulli potential, $B=u^2/2+h+\zeta$, during the incision. Like their experimental analogues in figure 5, these quantities show some tendency to be constant in space; that they are not perfectly so indicates the importance of unsteadiness and dissipation in the flow (cf. § 4.1). The theoretical dam break threshold on the (ϵ, A_0)-plane is presented in figure 8 (holding the other

parameters fixed), together with the number of seiches that are needed to initiate the dam break,

Qualitatively, the theoretical results reproduce many of the features in the experiments described in § 2; a more quantitative comparison demands the calibration of the theoretical parameters, which we attempt in § 5.2. One notable qualitative difference with the experiments arises because the model does not incorporate deposition. This feature is particularly non-physical in the initial phases of the dam break during which the overtopping waves decelerate due to drag once they reach the flat plane beyond the dam. At this stage, the eroded material should sediment from the relatively sluggish flow, leaving a skirt of deposition. Moreover, without deposition, there is no eventual arrest of erosion and the formation of a wedge-shaped relic of the original dam (see § 2); instead, the whole dam is removed.

4. A simpler model

In most situations, the rate of erosion is relatively slow, $\epsilon \ll 1$. Thus, as fluid rushes over the dam on the hydrodynamic time scale $\Delta/\sqrt{gZ_0}$, the bed remains largely in place and is only eroded over a longer time scale. Similarly, when the reservoir is much longer than the dam ($\ell \gg 1$) and empties through a shallow breach, the seiche period and drainage time are also relatively long. Hence, the problem decomposes into two parts: in the reservoir, a slow, large-scale seiche is superposed on a gradually changing mean level. The reservoir feeds water towards the dam, where the outflow steadily adjusts to the slowly varying upstream head and gradually erodes that obstruction. The mathematical expression of these ideas leads to a simpler model of the dam break.

4.1. *Dam hydraulics*

In the vicinity of the dam, we ignore fast hydrodynamic adjustments by neglecting the time derivatives h_t and u_t in comparison to $(hu)_x$ and uu_x. We also simplify the equations further by dropping the dissipative terms $(c_f|u| + \lambda)u/h$ and νu_{xx}, which brake the eroding outflow over the dam but do not qualitatively affect the dynamics (cf. Pratt 1986; Hogg & Hughes 2007). This reduces the system of equations (3.1)–(3.4) to

$$(hu)_x = \left(\frac{1}{2}u^2 + h + \zeta\right)_x = 0, \tag{4.1}$$

$$\zeta_t = -\epsilon E(u^2). \tag{4.2}$$

Equations (4.1) are familiar in hydraulics (e.g. Baines 1998) and imply that the water flux, q, and Bernoulli potential, B, are constant in space:

$$q(t) = hu,\ B(t) = \frac{1}{2}u^2 + h + \zeta. \tag{4.3}$$

Moreover, (4.1) can be expressed as the differential equation $(u - q/u^2)u_x = -\zeta_x$, which has no regular solution at the point at which $q = u^3$ unless ζ_x also vanishes there. Thus, if $\zeta(x_m) = \zeta_m$, $u(x_m) = u_m$ and $h(x_m) = h_m$ at the dam maximum $x = x_m$, it follows that

$$q = u_m^3, \qquad h_m = u_m^2 \qquad \text{and} \qquad B = \frac{3}{2}q^{2/3} + \zeta_m. \tag{4.4}$$

Sufficiently far upstream of the dam, $\zeta \to 0$, and the water level approaches that of the reservoir, denoted h_L. Hence, $B = h_L + q^2/(2h_L^2)$, and we arrive at an algebraic

problem determining the flow conditions at the maximum of the dam:

$$\left.\begin{aligned} &3q^{2/3} - q^2 h_L^{-2} = 2(h_L - \zeta_m), && \text{if } h_L > \zeta_m, \\ &q = u_m = h_m = 0, && \text{if } h_L < \zeta_m. \end{aligned}\right\} \tag{4.5}$$

The second line of (4.5) applies when the water level is lower than the top of the dam and when there is no outflow. The flow in the vicinity of the dam is therefore determined completely by the difference between the upstream water level and the dam maximum. In other words, the dam maximum 'hydraulically controls' the water flux (cf. Baines 1998). Finally, the dam erodes according to

$$\left(\frac{\partial \zeta}{\partial t}\right)_{x=x_m(t)} \equiv \frac{\mathrm{d}\zeta_m}{\mathrm{d}t} = -\epsilon E\left(u_m^2\right). \tag{4.6}$$

4.2. *The lake dynamics*

In the reservoir, $\zeta \to 0$, and we now retain the time derivatives in (3.1) and (3.2) because both the seiche and drainage are relatively slow. Let

$$\langle \ldots \rangle \equiv \frac{1}{\ell} \int_0^\ell (\ldots)\, \mathrm{d}x \tag{4.7}$$

denote the spatial average over the reservoir. Then the mean water depth is $H = \langle h \rangle$ and (from integrating (3.1) and applying the boundary conditions at $x = 0$) satisfies

$$\frac{\mathrm{d}H}{\mathrm{d}t} = -\frac{q}{\ell}, \tag{4.8}$$

where q is the water flux through the dam region, as given by (4.5).

A crude model for the seiche dynamics can be extracted using a Galerkin-style approximation based on the gravest linear mode: We set $h = H(t) + \eta(x, t)$ and average (3.1)$\times \cos(\pi x/\ell)$ and (3.2)$\times \sin(\pi x/\ell)$ over the reservoir. After a little manipulation,

$$\frac{\mathrm{d}}{\mathrm{d}t}\left\langle \eta \cos\left(\frac{\pi x}{\ell}\right)\right\rangle + \frac{\pi H}{\ell}\left\langle u \sin\left(\frac{\pi x}{\ell}\right)\right\rangle = \frac{1}{\ell}[(H+\eta)u]_{x=\ell} - \frac{\pi}{\ell}\left\langle \eta u \sin\left(\frac{\pi x}{\ell}\right)\right\rangle \tag{4.9}$$

and

$$\frac{\mathrm{d}}{\mathrm{d}t}\left\langle u \sin\left(\frac{\pi x}{\ell}\right)\right\rangle - \frac{\pi}{\ell}\left\langle \eta \cos\left(\frac{\pi x}{\ell}\right)\right\rangle = \left\langle \left[\nu u_{xx} - \frac{(\lambda + c_f|u|)}{(H+\eta)}u - u u_x\right] \sin\left(\frac{\pi x}{\ell}\right)\right\rangle. \tag{4.10}$$

The first term on the right of (4.9) represents an outgoing flux due to wave transmission across the dam. It is possible to make estimates of this term, but we neglect it here in the interest of simplicity. Finally, we take $\eta \ll H$ and compute the averages using the approximations

$$\eta \approx a(t)\cos(\pi x/\ell) \quad \text{and} \quad u \approx b(t)\sin(\pi x/\ell). \tag{4.11}$$

This furnishes a pair of equations for the modal amplitudes $a(t)$ and $b(t)$, which are quoted below and are coupled to the dam hydraulics via the upstream head, $h_L \equiv H - a$.

4.3. *The model*

The equations of the simplified model can be expressed in the compact form,

$$\frac{\mathrm{d}H}{\mathrm{d}t} = -\frac{u_m^3}{\ell}, \qquad \frac{\mathrm{d}\zeta_m}{\mathrm{d}t} = -\epsilon\left(u_m^2 - u_*^2\right)_+^\alpha, \tag{4.12}$$

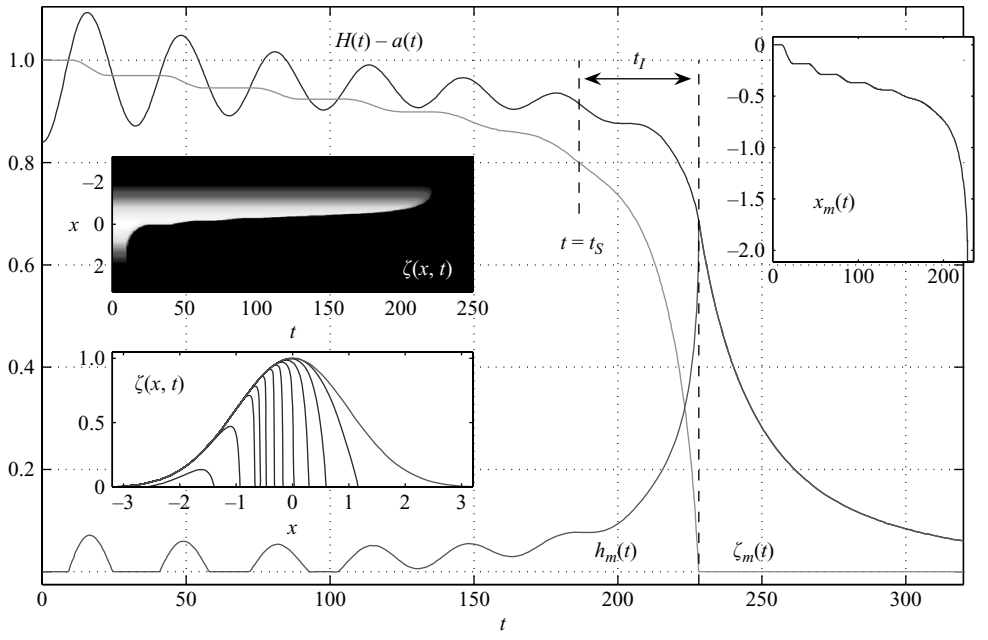

FIGURE 9. Solution of the reduced model, showing $H(t)-a(t)$, $\zeta_m(t)$ and $h_m(t)$ in the main picture, $x_m(t)$ in the inset on the right and two insets of $\zeta(x,t)$ on the left (snapshots for $t=0$, 10, 13, 17, 37, 63, 114, 165, 191, 204, 219 and 227 and as a density on the (t,x)-plane, with shading increasing uniformly from 0 to 1). The initial amplitude is $a(0)=0.124$, and the remaining parameter settings are as in figure 6.

$$\frac{\mathrm{d}a}{\mathrm{d}t}+\frac{\pi H}{\ell}b=0, \qquad \frac{\mathrm{d}b}{\mathrm{d}t}-\frac{\pi}{\ell}a=-\left(\frac{\pi^2\nu}{\ell^2}+\frac{\lambda}{H}+\frac{8c_f}{3\pi H}|b|\right)b, \tag{4.13}$$

where

$$u_m^2=\frac{2}{3}(H-a-\zeta_m)_+ +\frac{u_m^6}{3(H-a)^2}, \tag{4.14}$$

and the subscript $+$ on a variable X_+ is shorthand for $\mathrm{Max}(X,0)$, which conveniently incorporates the switching on and off of erosion and the flow over the dam. Note that (4.14) has multiple possible solutions in u_m, but only the solution continuously connected to $u_m=0$ at $H-a-\zeta_m=0$ is physically meaningful. Moreover, although the dam break dynamics are now described by the four variables (H, ζ_m, a, b), one must still solve (4.2) everywhere in order to compute the evolution of the full dam profile.

A sample solution is shown in figure 9 for an initial wave amplitude just above the threshold for dam break; the remaining parameter settings are the same as the numerical solutions of the full shallow-water equations displayed in figure 6. Although the reduced model qualitatively captures the dynamics of the full shallow-water system, the erosion is stronger in the reduced model, which can be attributed to the neglect of drag within the breach.

Thresholds on the (ϵ, A_0)-plane (with $A_0\equiv|a(0)|$) for the reduced model are shown in figure 10; the results qualitatively mirror those of figure 8. The figure includes a conservative estimate of the threshold obtained by first making the approximation $u_m^2\approx(2/3)(H-a-\zeta_m)$ in (4.14), which is valid when $u^2\ll h$ upstream of the dam. In

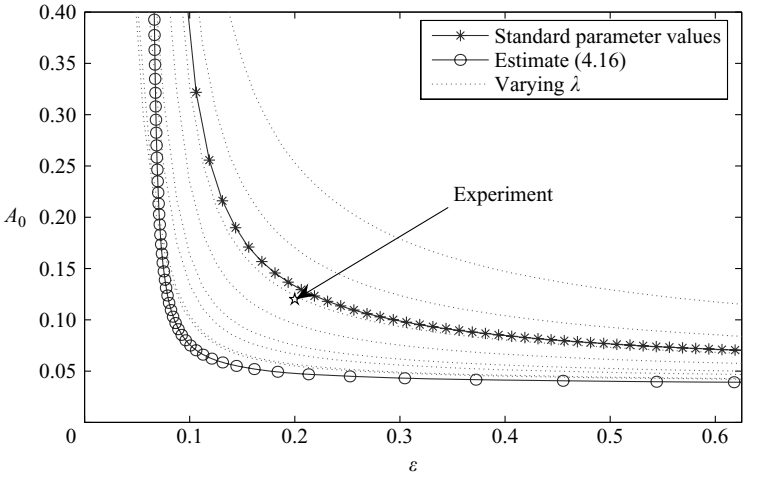

FIGURE 10. Dam break thresholds for the reduced model. Shown by the dotted lines are thresholds for different values of the drag parameter λ (the curves are for $\lambda = 0$, 10^{-4}, 0.001, 0.002, 0.005, 0.01, 0.02 and 0.04), with $c_f = 0$, $\nu = 0$. The other parameters are chosen as usual. The solid line and stars show the threshold for the 'standard' parameter settings of figure 6. The circles show the analytical prediction in (4.16). The star indicates the estimated experimental threshold, given the value of the erosion parameter determined in § 5.2.

this case, combining the equations in (4.12) gives

$$\frac{\mathrm{d}}{\mathrm{d}t}(H-\zeta_m) \approx \epsilon \left[\frac{2}{3}\left(H-a-\zeta_m-\frac{3}{2}u_*^2\right)_+\right]^\alpha - \frac{1}{\ell}\left[\frac{2}{3}(H-a-\zeta_m)_+\right]^{3/2}. \tag{4.15}$$

The right-hand side of (4.15) expresses the competition between erosion of the dam and drainage of the reservoir, as modulated by the seiche, and must be positive in order for a breach to occur. Moreover, since the maximum of $H-a$ over the period of the seiche is invariably less than $h_0 + A_0$ and decreases faster than ζ_m when the dam does not break, we estimate the threshold by demanding that the right-hand side of (4.15) be positive for the initial condition $H - a - \zeta_m = h_0 + A_0 - 1$, implying (on taking $\alpha = 3/2$)

$$\epsilon > \frac{(h_0 + A_0 - 1)_+^{3/2}}{\ell(h_0 + A_0 - 1 - 3u_*^2/2)_+^{3/2}}. \tag{4.16}$$

Figure 10 also shows how the threshold depends on the laminar friction coefficient λ and highlights how drag raises the actual amplitude threshold above the estimate in (4.16). Additionally the figure reports the experimental threshold based on the observations described in § 2 and the estimate of ϵ from § 5.2. Note that varying the other two dissipative parameters c_f and ν has much less affect on the threshold unless these parameters are given much larger values, reflecting the dominance of laminar drag in this physical regime.

4.4. *The incision*

Once the runaway incision begins, the seiche largely damps away, $(a, b) \to 0$, and (4.12) and (4.14) simplify to

$$\frac{\mathrm{d}H}{\mathrm{d}t} = -\frac{u_m^3}{\ell}, \qquad \frac{\mathrm{d}\zeta_m}{\mathrm{d}t} = -\epsilon\left(u_m^2 - u_*^2\right)_+^\alpha, \qquad u_m^2 = \frac{2}{3}(H-\zeta_m)_+ + \frac{u_m^6}{3H^2}, \tag{4.17}$$

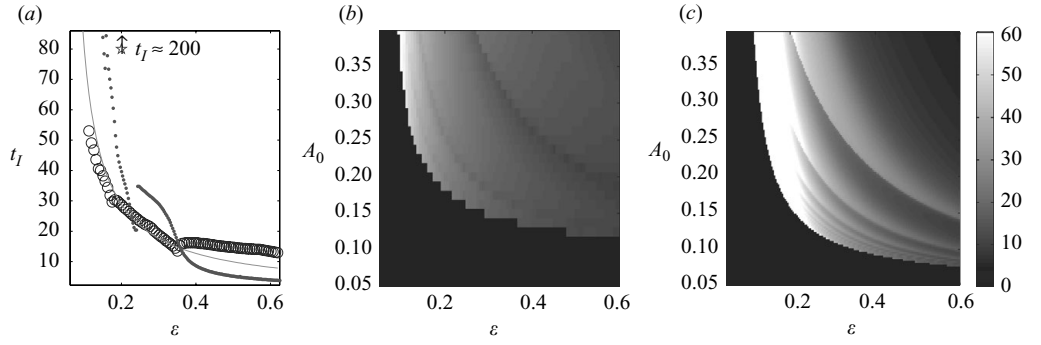

FIGURE 11. Runaway incision times, t_I, defined as the time taken from the moment that $\zeta_m = 0.8$ up to the instant that the dam is removed. Panel (*a*) shows the estimate in (4.18), together with measurements from the shallow-water model (circles) and the full reduced model (dots), computed for $A_0 = 0.3$. The star indicates the experimental measurement for the coarse sand dams, as given by the calibration of § 5.2. Panels (*b*) and (*c*) show t_I for the shallow-water model and full reduced model, respectively, as a density on the (ϵ, A_0)-plane (with standard parameter settings).

which also offers a model for dam breaks initiated by overfilling the reservoir. By simplifying (4.17) still further and assuming $\alpha = 3/2$, we may extract some analytical estimates of the time for the incision and maximum flux reached: Assuming that $u_m \approx \sqrt{2(H-\zeta_m)/3} \gg u_*$, we integrate (4.17) from the beginning of the incision $t = t_S$ (i.e. the time for the initial seiche) when $\zeta_m = \zeta_I$ and $H = H_I$, up to its end $t = t_S + t_I$ when $\zeta_m \to 0$. This gives a duration

$$t_I \sim \frac{C}{\epsilon}[1-(\epsilon\ell)^{-1}]^{-1}, \tag{4.18}$$

with

$$C = 2\left(\frac{3}{2}\right)^{3/2}\left\{(H_I-\zeta_I)^{-1/2} - \left[H_I - \frac{\zeta_I}{\epsilon\ell}\right]^{-1/2}\right\}. \tag{4.19}$$

By way of illustration, we adopt the convenient, if somewhat arbitrary choice $\zeta_I = 0.8$, and assume that the mean lake level has yet to decline appreciably at the beginning of the incision, so that $H_I \approx 1$. This leads to the incision time illustrated in figure 11. An even cruder approximation is to assume that $H_I - \zeta_I \ll 1$, giving $C \approx 2(3/2)^{3/2}(H_I - \zeta_I)^{-1/2} \approx 8$ (which leads to $t_I \approx 40$ for the dam break of figure 9). Also shown in figure 11 are analogous measurements of t_I from the full shallow-water and reduced models. The overall agreement is not especially good, partly because the estimate (4.18) is independent of the initial wave amplitude which retains some influence in the more complete models. However, the cruder estimates do reproduce the correct order of magnitude.

In both the shallow-water and reduced models, the maximum discharge, q_{max} (the greatest value of $|\mathrm{d}H/\mathrm{d}t|$), occurs at the end of the incision, when $t = t_S + t_I$ (cf. figure 9). At this instant, our approximation and integration of (4.17) implies

$$q_{max} = \frac{2}{3}\left[1 - \frac{\zeta_I}{\epsilon\ell}\right]^{3/2} \sim [1-(\epsilon\ell)^{-1}]^{3/2}. \tag{4.20}$$

The prediction (4.20) is plotted against ϵ in figure 12. Again we also include data for the full shallow-water and reduced models. Once more, the crude estimate fails to

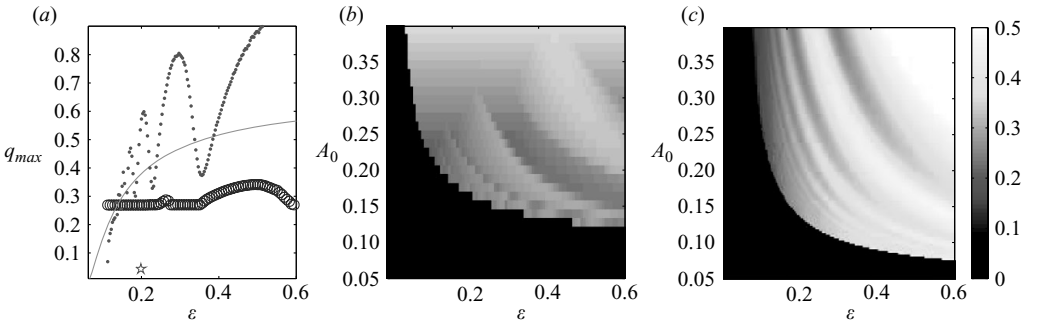

FIGURE 12. The maximum flux attained during the dam break, q_{max}. Panel (*a*) shows the estimate in (4.20), together with measurements from the shallow-water model (circles) and the full reduced model (dots), computed for $A_0 = 0.3$. The star indicates the experimental measurement for the coarse sand dams, as given by the calibration of § 5.2. Panels (*b*) and (*c*) show q_{max} for the shallow-water model and full reduced model, respectively, as a density on the (ϵ, A_0)-plane (with standard parameter settings).

incorporate any dependence on the initial wave amplitude, which is problematic for the full shallow-water model, as the maximum flux can be achieved in the reservoir during the seiches (leading to the relatively flat values of q_{max} as functions of ϵ), a feature also not captured by the reduced model.

After the incision has ceased, the lake drains away according to

$$H(t) = \left[H(t_S + t_I)^{-1/2} + \frac{(t - t_S - t_I)}{2\ell} \right]^{-2}, \tag{4.21}$$

which implies a characteristic, final drainage time scale $t_D \sim D\ell$, with D a factor of the order of unity.

5. Discussion

5.1. *Dimensional considerations*

The most important dimensionless groups of the theory are the combinations

$$A, \quad \epsilon \equiv Wg\Delta, \quad u_* = \frac{U_*}{\sqrt{gZ_0}}, \quad \lambda \equiv \frac{\Lambda\Delta}{Z_0\sqrt{gZ_0}}, \quad r = \frac{1}{\epsilon\ell} = \frac{1}{WgL}, \quad d = 1 - \frac{H_0}{Z_0},$$

which, respectively, control the initial wave amplitude, the rate of erosion, the erosion threshold, the fluid drag, the rate of lake drainage compared to erosion ($L = \Delta\ell$ is the dimensional lake length) and the initial difference between the mean lake level (H_0) and the dam height (Z_0). The parameters all play an important role in the initial seiche phase, and hence the threshold for dam break: A, λ, r and d determine the degree and persistence of overtopping, whilst ϵ and u_* set the amount of erosion. Dimensional analysis demands that the threshold may formally be written as the condition, $A > A_c(\epsilon, u_*, \lambda, r, d)$, and the results presented in §§ 3 and 4 offer some insight into the function A_c. Our crudest estimate suggests

$$A_c = d + \frac{2u_*^2}{3(1 - r^{2/3})} \equiv \frac{Z_0 - H_0}{Z_0} + \frac{2U_*^2}{3gZ_0} \left(1 - \frac{1}{(WgL)^{2/3}} \right)^{-1} \tag{5.1}$$

(cf. (4.16)). The physical interpretation is that the initial wave height should exceed the difference between the lake level and dam height by an amount given by the need

to surpass the erosion threshold and weighted by a factor which ensures that the erosion rate overtakes the competing effect of lake drainage ($WgL > 1$).

Likewise, the total time for the reservoir to empty is formally given by a function $t_B(A\ ,\epsilon,\ \lambda,\ r,\ d,\ u_*)\Delta/\sqrt{gZ_0}$. The dimensionless time scale t_B can be split into three components, $t_B = t_S + t_I + t_D$, where t_S is the time of the initial seiche; t_I is the time for the runaway incision to occur once initiated; and t_D is the final drainage time after the erosion of the dam has been arrested. Once the seiche initiates the runaway incision, the details of the initial lake and wave disturbance become secondary. Hence, we may write

$$t_B = t_S(A,\ \epsilon,\ \lambda,\ r,\ d,\ u_*) + t_I(\epsilon,\ r,\ u_*) + t_D(\epsilon r = \ell), \tag{5.2}$$

with t_I displayed in figure 11 and where our crudest estimates suggest that

$$t_I \sim \frac{C}{\epsilon(1-r)} \qquad \text{with} \qquad C \approx 8. \tag{5.3}$$

The peak discharge is

$$Q_{max} \sim Z_0\sqrt{gZ_0}\, q_{max}(A,\ \epsilon,\ u_*,\ \lambda,\ r,\ d), \tag{5.4}$$

where q_{max} is of the order of one (cf. figure 12). Our cruder estimates suggest (cf. also (4.20))

$$Q_{max} \sim Z_0\sqrt{gZ_0}\left(1 - \frac{1}{WgL}\right)^{3/2}. \tag{5.5}$$

5.2. *Comparing theory and experiment*

To compare theory and the experiments, one must first calibrate the empirical constants. The erosion model takes the form $\mathrm{d}\zeta_m/\mathrm{d}t = -WE(u_m)$. Consequently, by monitoring the dam height and water speed, one can measure the erosion parameter W once the threshold U_* in $E(u)$ is known. Following Parker (2006), for sediment with a single particle size, we express the threshold as a Shields stress,

$$\tau_* \equiv \frac{U_*^2}{Rg\delta} \approx 0.5\left[0.22Re_p^{-0.6} + 0.06\times 10^{-7.7Re_p^{-0.6}}\right], \tag{5.6}$$

where

$$Re_p = \frac{(Rg\delta)^{1/2}\,\delta}{\nu} \tag{5.7}$$

is the particle Reynolds number; $R = (\rho_s - \rho)/\rho$; and ρ_s and δ are the particle density and mean diameter (with ρ as the fluid density and ν as the fluid kinematic viscosity). Proceeding down this route for the coarse sand, we arrive at the estimates, $Re_p \approx 100$ and $U_* \approx 0.015\,\mathrm{m\ s^{-1}}$. This threshold speed is much less that the observed flow speeds over the dam's crest (see figure 5), and so $W \approx u_m^{-3}(\mathrm{d}\zeta/\mathrm{d}t)$ (using $\alpha = 3/2$). Thence, we estimate that $W \approx 0.26 \pm 0.1\,\mathrm{s^2\,m^{-2}}$ for experiments in the narrow tank and $W \approx 0.15 \pm 0.1\,\mathrm{s^2\,m^{-2}}$ for the wide tank, which are consistent and suggest we adopt the nominal value $W = 0.2\,\mathrm{s^2\,m^{-2}}$. The erosion parameter, W, and threshold, U_*, then translate to the estimates, $\epsilon = gW\Delta \approx 0.2$ and $u_*^2 = U_*^2/(gZ_0) \approx 10^{-4}$ (with $Z_0 \approx 0.1\,\mathrm{m}$ and $\Delta \approx 0.1\,\mathrm{m}$). An analogous calculation for the bimodal mixtures cannot be made, since formulae equivalent to (5.6) do not exist for such materials. There is also a certain amount of disagreement in the literature over formulae such as (5.6) (e.g. Ouriemi *et al.* 2007). We do not regard this issue as significant because the flow speeds reached in the breach are well above threshold.

The primary damping of the seiche in the experiments arises through viscous dissipation in Stokes' layers adjacent to the walls of the tank. The effective damping rate can be estimated to be of the order

$$\Lambda \approx \left(\frac{\pi^2 \nu_T^2 g}{4L^2 H_0^3} \right)^{1/4} \sim 0.01 \text{ s}^{-1}.$$

Hence, $\lambda = \Lambda \Delta / Z_0 \sqrt{g Z_0} \sim 0.01$. Given that $\Delta / Z_0 \sim 1$, the estimates of C_f, which range from 0.001 for smooth walls to 0.1 for rough ones, translate to $c_f \approx 0.001$–0.1. Finally, the viscous coefficient, ν, would be of the order of 10^{-5} if the molecular value of viscosity were appropriate but could be as large as 10^{-2} if this quantity parameterized turbulent eddies with characteristic speeds of 0.1 m s^{-1} and length scales of 0.01 m (suggesting an effective kinematic viscosity of $10^{-3} \text{ m}^2 \text{ s}^{-1}$).

For comparison, we also mention a cursory calibration for the geological setting: data from the Nostetuko Lake outburst flood (Clague & Evans 2000) indicate that the moraine dam was incised at a rate of approximately 10 m h^{-1} by a flow with velocity 3.3 m s^{-1}, suggesting $W = O(10^{-4}) \text{ s}^2 \text{ m}^{-2}$. Assuming a dam width and height $O(100)$ m, $\epsilon = O(10^{-1})$. The lake length was order a kilometre, indicating $\ell \sim 10$. Turbulent drag surely dominates laminar friction in this situation, and so we expect drag to be given by the Chézy form with $C_f \approx 0.1$ (taking $\Delta \sim Z_0$).

The calibration therefore suggests parameter settings that are similar to the standard values adopted for most of our theoretical calculations. Moreover, in view of the crudeness of the theory, the large number of parameters and the omission of several physical effects that clearly play a role (such as deposition), it is questionable to fine-tune the parameter settings any further. Hence we compare the two without further adjustment.

For A_c, the theoretical models suggest that the threshold in initial wave amplitude should be about 13 % of the water depth, which is remarkably close to the observation reported in § 2 (see also figure 8). Crude estimates of the experimental incision time and maximum flux can be extracted from the time series of lake level shown in figure 3 and are of the order of 20 s and $2.4 \times 10^{-3} \text{ m}^2 \text{ s}^{-1}$, respectively ($q \approx -L \mathrm{d}h_L/\mathrm{d}t$). Direct measurements of the flux within the breach using tracer particles are higher ($4 \times 10^{-3} \text{ m}^2 \text{ s}^{-1}$ or more, see figure 5). Theory predicts a dimensionless time for incision of the order of 30 (see figure 11). Coupled with the characteristic time scale, $\Delta / \sqrt{g Z_0} \sim 0.1$ s, used in the non-dimensionalization, this corresponds to a time of about 3 s. The corresponding maximum flux from (5.5) is $3.5 \times 10^{-2} \text{ m}^2 \text{ s}^{-1}$. Hence, theory and experiment compare less favourably for the incision time and maximum flux (see also figures 11 and 12). The theoretical predictions are sensitive to the material properties and in particular on the estimate of $r = 1/(WgL)$. Further, the theoretical estimates may be poor due to the omission of deposition, which plays a key role in arresting erosion in the later stages of the experimental dam breaks. Alternatively, we have also ignored the feedback of the sediment on the flow dynamics and in particular the eroded mass added to the flow, which could reduce the flux and lengthen the duration of the dam break.

6. Conclusions

In this paper, we have modelled, both experimentally and theoretically, how a dam can be broken by a combination of overtopping waves and runaway erosional incision. The experiments demonstrate the feasibility of the scenario, and the phenomenology can be qualitatively reproduced by theoretical models. Perhaps

unsurprisingly, the comparison fares less favourably at the quantitative level, although a fine-tuning of parameters and the addition of more physics of sediment transport may improve the situation. The ingredients of the models include a slowly decaying seiche in the dammed reservoir that feeds water to a hydraulically controlled breach in the dam. Whether the model incorporates these ingredients within a shallow-water formulation or in a simpler conceptual model capturing the main global variables (dam height, reservoir depth and seiche amplitude), the dam break process amounts to a competition between erosion, lake drainage and seiche damping. A threshold naturally results, wherein the initial wave amplitude, or rate of erosion, should exceed a critical value for a break to occur.

A key limitation of our theoretical analysis is that it is two-dimensional, whereas moraine-dammed lakes are complicated three-dimensional structures. In fact, a puzzling observation in the experiments is that discharges are comparable in both narrow (5 cm width) and wide (20 cm width) tanks (see figure 3), and the width of the incised channels in the latter appears unimportant. Theoretical computations with the three-dimensional generalization of the shallow-water model (Balmforth *et al.* 2008) also suggest that discharges, and even the erosion threshold, are weakly sensitive to the third dimension. This result can be rationalized by the fact that, for steady flow in a three-dimensional channel of slowly varying width, the concept of hydraulic control still applies but to the cross-channel averaged flow speed and depth (e.g. Baines 1998). Consequently, the difference between the breadth of the lake and the width of the breach in the dam does not play a role, as might have originally been thought. More generally, one expects that the ratio of lake breadth to breach width becomes important when the lake is much wider than the incision. In our experiments and shallow-water computations, the breach is only three or so times narrower than the lake width. In geological settings, the lake could be rather wide and the argument less compelling. Furthermore, other physical effects, such as the focusing of the initial wave into a narrow pre-existing channel (Blown & Church 1985), might dominate the phenomena studied here.

We thank Antonello Provenzale for the negative remarks that helped to drive this work forward. The experiments were conducted at the Coastal Research Laboratory, Woods Hole Institute of Oceanography, during the 2006 Geophysical Fluid Dynamics Summer Study Program (which was supported by the National Science Foundation). We thank Keith Bradley for assistance with the experiments and the participants at Walsh Cottage for discussions.

REFERENCES

Baines, P. 1998 *Topographic Effects in Stratified Flows.* Cambridge University Press.

Balmforth, N. J., von Hardenberg, J., Provenzale, A. & Zammett, R. 2008 Dam breaking by catastrophic erosional incision. *J. Geophys. Res.* **113**, F01020. Doi:10.1029/2007JF000756.

Blown, I. G. & Church, M. 1985 Catastrophic lake drainage within the Homathko river basin, British Columbia. *Can. Geotech. J.* **22**, 551–553.

Cao, Z., Pender, G., Wallis, S. & Carling, P. 2004 Computational dam-break hydraulics over erodible sediment bed. *J. Hydr. Engng ASCE* **130**, 689–703.

Clague, J. J. & Evans S. G. 2000 A review of catastrophic drainage of moraine-dammed lakes in British Columbia. *Quart. Sci. Rev.* **19**, 1763–1783.

Clarke, G. K. C. 1987 Subglacial till: a physical framework for its properties and processes. *J. Geophys. Res.* **92** (B9), 9023–9036.

Coleman, S. E., Andrews, D. P. & Webby, M. G. 2002 Overtopping breaching of noncohesive homogeneous embarkments. *J. Hydr. Engng ASCE* **128**, 829–838.

Cui, Y., Parker, G., Braudrick, C., Dietrich, W. E. & Cluer, B. 2006*a* Dam Removal Express Assessment Models (DREAM). Part 1. Model development and validation. *J. Hydr. Res.* **44**, 291–307.

Cui, Y., Braudrick, C., Dietrich, W. E., Cluer, B. & Parker, G. 2006*b* Dam Removal Express Assessment Models (DREAM). Part 2. Sample runs/sensitivity tests. *J. Hydr. Res.* **44**, 308–323.

Hogg, A. M. & Hughes, G. O. 2006 Shear flow and viscosity in single-layer hydraulics. *J. Fluid Mech.* **548**, 431–443.

Hubbard, B., Heald, A., Reynolds, J. M., Quincey, D., Richardson, S. D., Luyo, M. Z., Portilla, N. S. & Hambrey M. J. 2005 Impact of a rock avalanche on a moraine-dammed proglacial lake: Laguna Safuna Alta, Cordillera Blanca, Peru. *Earth Surf. Processes Landforms* **30**, 1251–1264.

Keulegan, G. H. 1959 Energy dissipation in standing waves in rectangular basins. *J. Fluid Mech.* **6**, 33–50.

McKillop, R. J., & Clague, J. J. 2007 A procedure for making objective preliminary assessments of outburst flood hazard from moraine-dammed lakes in southwestern British Columbia. *Nat. Hazards* **41**, 131–157.

McKillop, R. J., & Clague, J. J. 2007 Statistical, remote-sensing based approach for estimating the probability of catastrophic drainage from moraine-dammed lakes in southwestern British Columbia. *Global Planet. Change* **56**, 153–171.

Merkin, J. H. & Needham, D. J. 1986 An infinite period bifurcation arising in roll waves down an open inclined channel. *Proc. R. Soc. Lond.* **405**, 103–116.

Needham, D. J. & Merkin, J. H. 1984 On roll waves down an open inclined channel. *Proc. R. Soc. Lond.* A **394**, 259–278.

Ouriemi, M., Aussillous, P., Medale, M., Peysson, Y. & Guazzelli, E. 2007 Determination of the critical Shields number for erosion in laminar flow. *Phys. Fluids* **19**, 061706.

Parker G. 2006 1D sediment transport morphodynamics with applications to rivers and turbidity currents. http://cee.uiuc.edu/people/parkerg/morphodynamics_e-book.htm.

Pratt, L. J. 1986 Hydraulic control of sill flow with bottom friction. *J. Phys. Oceanogr.* **16**, 1970–1980.

Rabassa, J., Rubulis, S. & Suarez, J. 1979 Rate of formation and sedimentology of (1976-1978) push-moraines, Frias Glacier, Mount Tronadoz (41°10′S; 71°53′W), Argentina. In *Moraines and Varves: Origins, Genesis, Classification*, (ed. C. Schluchter), Balkema, pp. 65–79.

Rickenmann D. 2001 Comparison of bed load transport in torrents and gravel bed streams. *Water Resour. Res.* **37**, 3295–3305.

Taki, K. & Parker, G. 2004 Transportational cyclic steps created by flow over an erodible bed. Part 2. Theory and numerical simulation. *J. Hydraulic Res.* **43** (5), 502–514.